JGR Space Physics

RESEARCH ARTICLE
10.1029/2023JA031422

Ionospheric and Atmospheric Response to Extremely Severe Cyclonic Storm Nida of 29 July–02 August 2016

Sanjay Kumar[1,2], **Wu Chen**[2], **and Osei-Poku Louis**[2]

[1]Department of Physics, Nehru Gram Bharti (Deemed To Be University), Prayagraj, India, [2]Department of Land Surveying and Geoinfromatics, The Hong Kong Polytechnic University, Hong Kong, China

Key Points:

- Enhanced atmospheric ozone is observed during cyclone attributed to enhanced lightning activity which may be source of NOx
- Magnitude of ionospheric perturbation observed along left/right to cyclone track are significantly differ
- Strong scintillation activity compared to normal days from ground and satellite based data are observed during the cyclone period

Correspondence to:
S. Kumar,
sanjay.skitvns@gmail.com

Citation:
Kumar, S., Chen, W., & Louis, O.-P. (2023). Ionospheric and atmospheric response to extremely severe cyclonic storm Nida of 29 July–02 August 2016. *Journal of Geophysical Research: Space Physics*, *128*, e2023JA031422. https://doi.org/10.1029/2023JA031422

Received 22 FEB 2023
Accepted 5 OCT 2023

Abstract Tropical cyclones are one of the biggest threats to life and property. During cyclone period storm surge, flooding, extreme winds, tornadoes and lighting cause significant impacts on life and property and hence affects life of human being to a great extent. Nida was the third tropical cyclone requiring the issuance of tropical cyclone warning signals by the Hong Kong Observatory in 2016 and maximum hourly mean winds of 158 km/hr was recorded in Hong Kong. It affected many cities of China and about 500,000 people, more than 300 houses collapsed and made economic loss of about 500 million RMB. Investigation of lightning discharges around the cyclone track line revealed that the strong lightning activity is noticed during the cyclone period with a super lightning maxima on 30 July and 01 August. The effect of this typhoon on the ionosphere is studied using the TEC data from GPS measurements taken around the cyclone track and satellite based COSMIC measurements. Strong convective activity which is driver for the thunderstorm and gravity waves activity noticed from the negative cloud top temperature as low as −50°C observed from AIRS satellite during the cyclone period. Significant enhancement is atmospheric ozone is observed during the cyclone period which could be attributed to thunderstorm activity present during the cyclone period. The analysis found decrease in GPS-TEC data at stations around Hong Kong region during the landfall of the cyclone. The magnitude of perturbation in TEC is found larger at stations lying toward right/eastward of the cyclone track as compared to those in the left/westward from the cyclone track. In addition, periodic signatures in ionospheric TEC data were also detected. Continuous wavelet transform to DTEC data has been made to estimate period and found the periodic structure in ionospheric TEC belongs to AGWs with period 9–20 min and frequency 1–2 mHz. Strong scintillation activity as high as S4-index 1.35 from GPS measurements has been noticed at Sanya station during cyclone period on 02 August which is further confirmed by satellite based measurements from COSMIC. Both measurements show maximum scintillation activity during 1400–1600 UT. The strong scintillation activity as compared to normal days observed during the cyclone period is attributed to lightning induced electric filed as well as generation of AGWs due to deep convection which could act as seed perturbation for generation of ionospheric irregularities by Rayleigh-Taylor instability mechanism.

1. Introduction

Ionosphere plays a very important role in communication and navigation services and show a high degree of variability. In addition to solar and geomagnetic disturbances ionosphere is also affected by forcing from above and below from it. Atmospheric effects on the ionosphere such as solar eclipse, thunder storm, cyclones, typhoon, and stratospheric warming events, etc. have proven ability to perturb ionosphere to a great extent and have become a new topic of study in recent years (Cairo et al., 2008; Immel et al., 2009; Isaev et al., 2006; Shen, 1982). Deep tropical convection, mesoscale convective complexes (MCCs), Tropical cyclones (TCs), typhoons, tornadoes, thunderstorms, upper troposphere jet, etc., are some of the disturbances of tropospheric meteorological origin, which are believed to cause this ionospheric perturbation. The coupling between the ionosphere and the underlying atmosphere is proposed to be linked through different channels: (a) upward propagating waves in the neutral atmosphere, (b) atmospheric DC electric field, (c) lighting-generated electric field, and (d) neutral particle dynamics, due to underlying large-scale weather systems originating from the surface or upper troposphere (Forbes et al., 2000; Isaev, Sorokin, Chmyrev, Serebryakova, & Ovcharenko, 2002, Isaev, Sorokin, Chmyrev, Serebryakova, & Yaschenko, 2002; Lastovicka, 2006; Shao et al., 2013; Sorokin & Cherny, 1999; Sorokin et al., 2005). Using foF2 data over 100 ionosonde stations, Forbes et al. (2000) confirmed that under geomagnetic quiet conditions meteorological influence to ionospheric variability is approximately ±25%–35% at "high frequencies" (periods of a few hours to 1–2 days) and approximately ±15%–20% at "low frequencies" (periods

of approximately 2–30 days) about the mean of ionospheric variability, at all latitudes. In recent years Cyclone activity in lower atmosphere produces atmospheric perturbations which can be observed in several parameters such as ozone (Cairo et al., 2008; Das et al., 2016), NOx (Naik et al., 2008), lightning activity (Dube et al., 2020), rainfall etc.

The solar activities have significant effects on the ionospheric electron density distribution and hence total electron content from the upper part. In recent years' atmospheric layers lying below the ionosphere have also been known to affect significantly the ionospheric variability (Vadas & Azeem, 2021). In addition, earthquakes, solar eclipse, thunderstorms/lightning, cyclone activity in the lower atmosphere also affect the ionospheric electron density distribution and plasma bubble occurrences in the ionosphere through gravity waves generation which have been reported in previous papers (Dube et al., 2020; Kumar et al., 2017; Li et al., 2022; Tang et al., 2019). During last decades several reports have been published to notice about atmospheric gravity waves (AGWs) generated from low-pressure cyclonic system. The GWs generated during cyclone transfers their energy and momentum to upper atmospheric layers which further affects thermal structure, composition changes in middle and upper atmosphere and global circulation (Fritts & Alexander, 2003). The AGWs couple with the Earth's atmosphere-ionosphere system and create perturbations in different layers: D, E, and F regions of the ionosphere (e.g., Collier et al., 2006; Guha et al., 2016; Immel et al., 2009; Kuo & Lee, 2015; Lay et al., 2015; Takahashi et al., 2009). However, the basic process of GWs propagation from lower atmosphere/troposphere to the thermosphere/ionosphere is not completely understood till now because it is challenging problem for scientific community to constrain propagation process using observations. In this study, which is first of its kind from Phillipines Ocean sector, concentrates on study of ionospheric TEC perturbations, Plasma bubble occurrences/scintillation associated with a very severe cyclonic storm Nida of July–August 2016. Generation and propagation of Gravity waves have been studied by detecting its signature in ionospheric TEC data. The characteristics of GWs using GPS-TEC data have also been analyzed using Savitzky-Golay filter technique. The method of data analysis is written in Section 2, results and discussion in Section 3. Finally, Section 4 will conclude the finding of this study.

2. Data and Method of Analysis

In this study GPS observation data around cyclone track has been used to estimate slant total electron content (STEC) which is further converted in to vertical total electron content (VTEC) using mapping function and discussed elsewhere (Rama Rao et al., 2006). The VTEC data estimated is further used to study ionospheric perturbation during the cyclone period.

The rate of change of TEC index (ROTI) is the standard deviation of rate of change of TEC (ROT) and ROTI is normally used to observe the ionospheric perturbation which indicates presence of ionospheric irregularities/plasma bubbles (Pi et al., 1997; Tang et al., 2021). ROTI is computed from ROT data over 5 min interval. To compute ROTI from TEC data having sampling of 0.5 min from the following equations are used

$$\mathrm{ROTI} = \sqrt{\langle \mathrm{ROT}^2 \rangle - \langle \mathrm{ROT} \rangle^2}$$

The ROT in above relation can be computed from TEC data and ROT at epoch t_j is given by following relation

$$\mathrm{ROT}\,(t_j) = \frac{\mathrm{TEC}(t_j) - \mathrm{TEC}(t_{j-1})}{t_j - t_{j\text{-}1}}$$

The ROT is expressed in TECU/min; where 1 TECU = 10^{16} electrons m^{-2}.

The cloud top temperature is an indicator of development of convective system which can be derived from AIRS (Atmospheric Infrared Sounder) satellite and downloaded from GIOVANI. This is one of the three sensors on board Aqua that is capable of providing estimates of water vapor and other met parameters in the atmosphere (Parkinson, 2003). In this study daily daytime ascending surface temperature (AIRS3STD_V06) with spatial resolution $1° \times 1°$ is taken from GIOVANI, NASA interfaced at website giovani.nasa.gov.in.

The Total Ozone Mapping Spectrometer (TOMS) was a NASA satellite instrument, specifically a spectrometer, for measuring ozone values. The ozone concentration in terms of total ozone column (TOC) daily data product with $1° \times 1°$ resolution can be downloaded from GIOVANI website interfaced at https://giovanni.gsfc.nasa.gov/giovanni/.

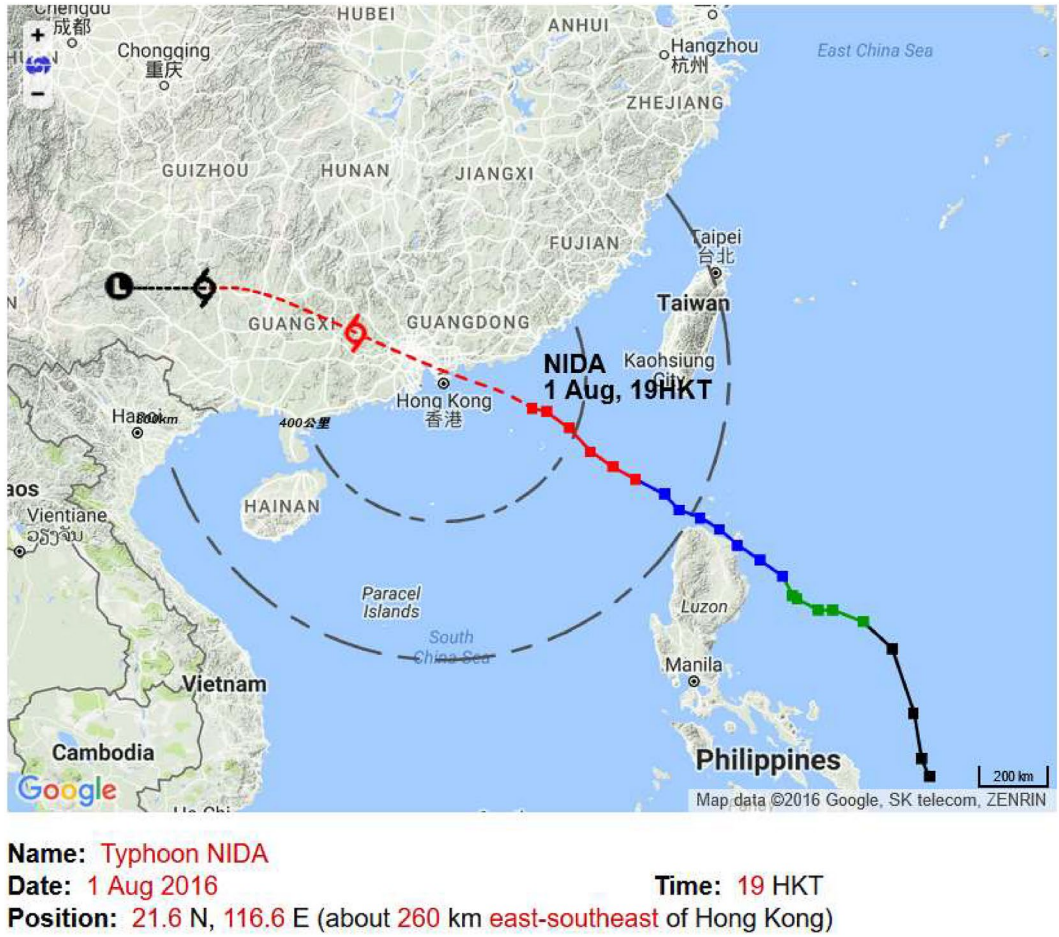

Figure 1. Trajectory of cyclone showing it origin on 29th July and movement toward Hong Kong.

2.1. Typhoon Nida (1604): 29 July–3 August 2016

Nida was the third tropical cyclone necessitating the issuance of tropical cyclone warning signals by the Hong Kong Observatory in 2016. It was also the first tropical cyclone requiring the issuance of Gale or Storm Wind Signal No. 8 in the year. Typhoon Nida was formed as a tropical depression over the western North Pacific about 750 km east-southeast of Manila (Philippines) on the night of 29 July 2016 and moved north-north-westwards at first. Nida then took on a north-westerly track toward the Luzon Strait on the afternoon of 30 July and intensified gradually. After developing into a severe tropical storm on the morning of 31 July, it swept across the north coast of Luzon in the afternoon and entered the north eastern part of the South China Sea that night, taking on a west-north westerly track toward the coast of Guangdong. It further intensified into a typhoon and reached its peak intensity on the afternoon of 01 August with an estimated sustained wind speed of 130 km/hr near its center. Nida made landfall near Dapeng Peninsula around 3 a.m. On 02 August and moved across Shenzhen, passing just to the north of Hong Kong. It continued to weaken as it moved further inland, before finally degenerating into an area of low pressure over Guangxi early in the morning of 03 August (Figure 1). Due to NIDA about 500,000 people were affected and more than 300 houses collapsed in Guangdong, Guangxi, Hunan, Guizhou and Yunnan during the passage of Nida, with direct economic loss exceeding 500 million RMB (https://www.hko.gov.hk/en/publica/tc/tc2016/section3_3rpt.htm).

To have knowledge about development of convective activity (driver of the thunderstorm) spatial distribution of cloud top temperature derived from the AIRS satellite is shown in Figure 2. From this figure negative cloud top temperature is noticed during the cyclone period which was found minimum of ∼−50°C on 02 August. The pronounced negative top temperature observed around cyclone track is an indicator of development of convective

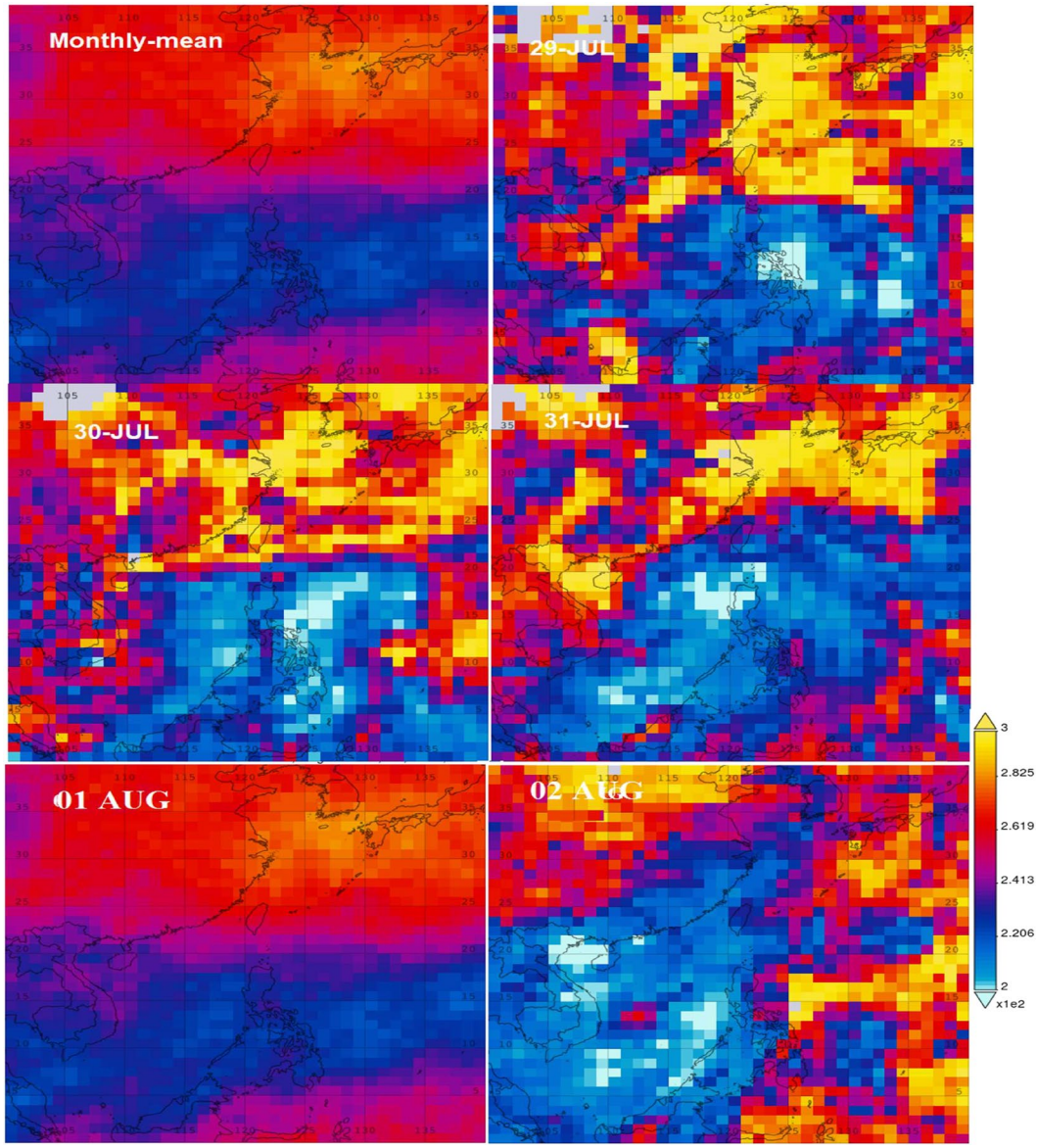

Figure 2. Map showing spatial distribution cloud top temperature (°K) during 29 July −01 August and its comparison with monthly mean of August 2016. Pronounced negative temperature as low as −50°C during land fall of cyclone in Hong Kong and surrounding region on 02 August is an indication of formation of convective system.

system and hence the thunderstorm activity. Moreover, the development of the convective activity is an important source for generation of atmospheric gravity waves (Fritts & Nastrom, 1992; Nastrom & Fritts, 1992).

3. Results and Discussion

3.1. Perturbation in Atmospheric Ozone

The stratospheric ozone (O_3) layer, found around 25–30 km altitude regulates the amount of ultraviolet radiation coming from the Sun to the Earth's surface. Therefore, ozone is an important greenhouse gas, which acts as an oxidant in the troposphere and has an important role in climate forcing and therefore have significant impacts on human health and life. Figure 3 shows variation of atmospheric ozone (total ozone column) taken from TOMS satellite. From figure significant enhancement in total ozone column is noticed during the cyclone period from 29 July to 01 August. The thunderstorm and lightning discharges are expected to be major sources of NOx and

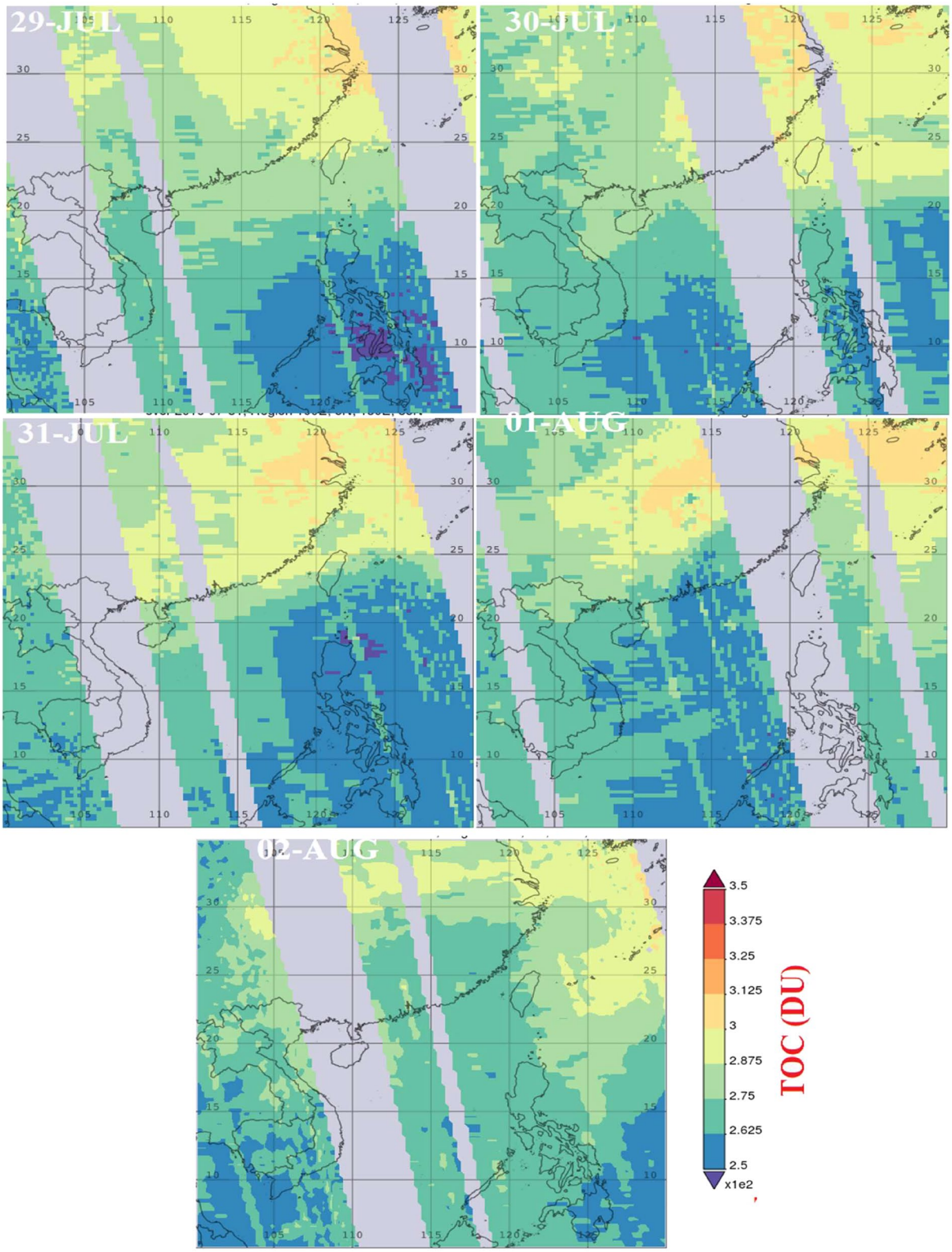

Figure 3. Variation of total ozone column (DU) during 29 July–02 August 2016. Significant enhancement in ozone has been observed during the cyclone period indication formation of convective system and lightning activity.

concentration of NOx may affect the ozone concentration in the atmosphere through chemical reactions. The high concentration of NOx present in the atmosphere noticed during the cyclone period from 29 to 31 July.

In general, over the middle and higher latitudes, stratospheric-air intrusion into the troposphere is prominent which are also linked with synoptic scale disturbances including cyclone activities (e.g., Stohl et al., 2003). This downward air flow is attributed to the dissipation of extra-tropical planetary and gravity waves in the stratosphere (Holton et al., 1995). The downward flows from the stratosphere to the troposphere is continuous and in a much smaller timescale over the extratropics (Bourqui & Trepanier, 2010; Stohl et al., 2003). As for as global ozone budget is concerned about 25%–50% of tropospheric ozone sources are from middle-latitude stratospheric disturbances (Bourqui & Trepanier, 2010; Das et al., 2016). Since limitation of this paper is that we are using TOC which cannot reflect contribution from different atmospheric layers so these processes of tropospheric enhancement are not significant and vertical altitude profile of atmospheric ozone will reflect better picture. Since, the effect of Coriolis force over mid and high latitude is more significant as compared to equatorial and tropical region which deflects the wind toward eastward/westward in the Northern/Southern hemisphere therefore spatial and vertical distribution of ozone is required for further investigation (Lutgens & Tarbuck, 2013).

It is important to note that minor neutral components play a significant role in processes controlling the ionization balance in the mesosphere/lower D-region of the ionosphere through chemical reactions including ozone concentration (Osepian & Dalin, 2009). The knowledge of altitude profile of ozone is important in determining effective recombination coefficient (recombination rate) and hence the electron density profile in the lower part of D-region (Osepian & Dalin, 2009). In addition ozone shadowing in short wavelength solar UV flux from the D-region ionosphere due to stratospheric ozone absorption also affects VLF sunrise phase perturbation (SPP) variations propagating in D-region of the ionosphere. Further Macotela et al. (2019) have shown that variation in atmospheric ozone number density at altitudes 38–42 km are better correlated ($R = 0.70$) with the size of SPP, the correlation with ozone is higher than that of atmospheric temperature.

3.2. Perturbation in TEC Data

Figure 4 shows time series of lightning discharges including lightning count of +CG, −CG and total lightning count along with lightning peak current (kA) respectively from top to bottom in 1 hr interval from 29 July to 03 august 2016. From the histogram it is seen that strong lightning activity is noticed during the period with a evidence of super lightning which were observed on 30 July and 01 august having lightning count ≥40,000.

To study the effect of cyclone on ionospheric TEC, we have selected 12 GPS stations lying along, left and right to the cyclone track. Since few stations are very closely spaced so their locations cannot be seen clearly and listed in Table 1. Figure 5 shows the cyclone track marked by red circle from 29 July to 04 August. The selected GPS stations lying along, left/right to cyclone track are marked by * with red color and each GPS station is rounded by blue circle. The geographical locations of GPS stations are also mentioned in Table 1. The ionospheric electron density distribution is significantly affected by the solar and geomagnetic activity. So before discussing effect of cyclonic storm on ionosphere it is important to note the Dst index during the cyclone period from 29 July to 02 August >−18 nT. This suggest that the cyclone period is completely free from the geomagnetic activity and period is geomagnetic quiet (Polyakova & Perevalova, 2011). The variation in sunspot number and solar flux during the period are respectively from 71 to 75 and 73 to 77 sfu (https://omniweb.gsfc.nasa.gov/form/dx1.html). So our analysis period is free from solar and geomagnetic disturbances and most favorable for studying the effects of tropical cyclone on the state of the ionosphere. Figure 6 shows variation of TEC data during the cyclone period along with TEC during geomagnetic quiet days without cyclone of the month at selected GPS stations lying around the cyclone track. The TEC data during cyclone period have been compared with those days without cyclone. It is to be noted that on 29 July enhancement in TEC is noticed at PPPC, PIMO, PTAG, TNML, GUAM, GUUG, CKSV, SMST stations and reduction at PGEN station. The PGEN station lies in southward direction from the cyclone origin whereas other stations lie in northward. Two stations WUHN and SMST are at similar latitude but TEC at SMST station which is situated on right side/eastward of cyclone track, show larger enhancement. On 30 July most of the stations show enhancement in TEC except GUAM station which reveals depression in TEC data. On 31 July depression in TEC is observed at most of the station except only GUUG, CKSV, WUHN, TNML. On 01 August depression in TEC is also noticed at all station except HKSL, HKWS, and WUHN. On 02 august enhancement is TEC data is observed at all the station except only GUAM station which is lying in eastward of cyclone track.

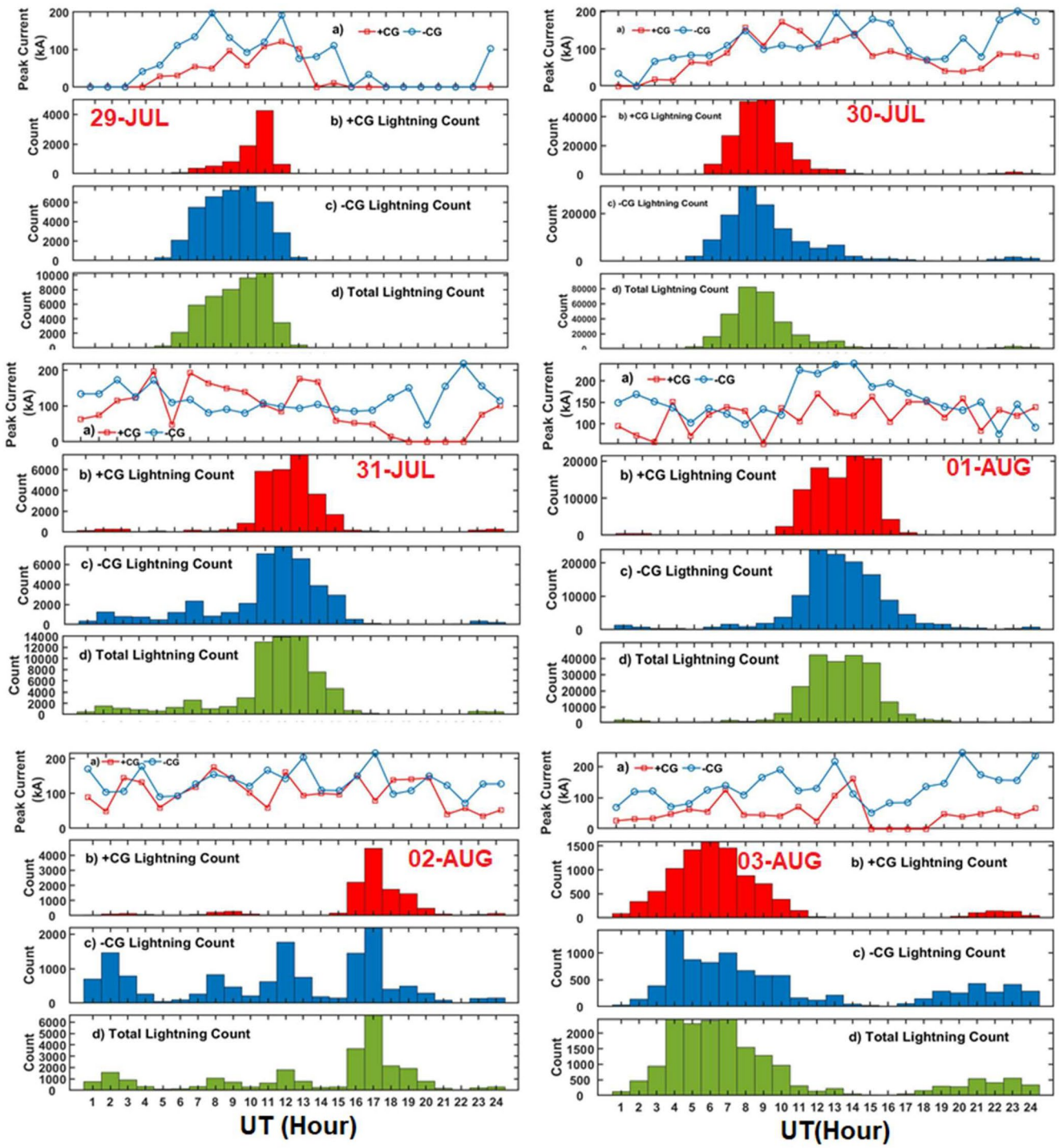

Figure 4. (a–d) Time series of lightning peak current along with histograms of lightning counts due to +CG, −CG, and total respectively from top to bottom during 1 hr interval. Each block represents plots for a day from 29 July to 03 August 2016. From the histogram strong lightning activity is observed during the period with super lightning on 30 July and 01 August (lightning count ≥40,000).

In this study perturbation in the ionosphere that is, increase and decrease in TEC has been observed during the cyclone period. The observed perturbation in ionosphere may be the combined effect of cyclone induced gravity waves which may propagate up to the ionosphere, ejection of neutral particles from the terminator of cyclone. The TC induced perturbations in the ionosphere such as local plasma density perturbations, appearance of electric filed, ELF/VLF zone development are possible due to injection of stream of neutral particles from lower atmospheric altitude to the

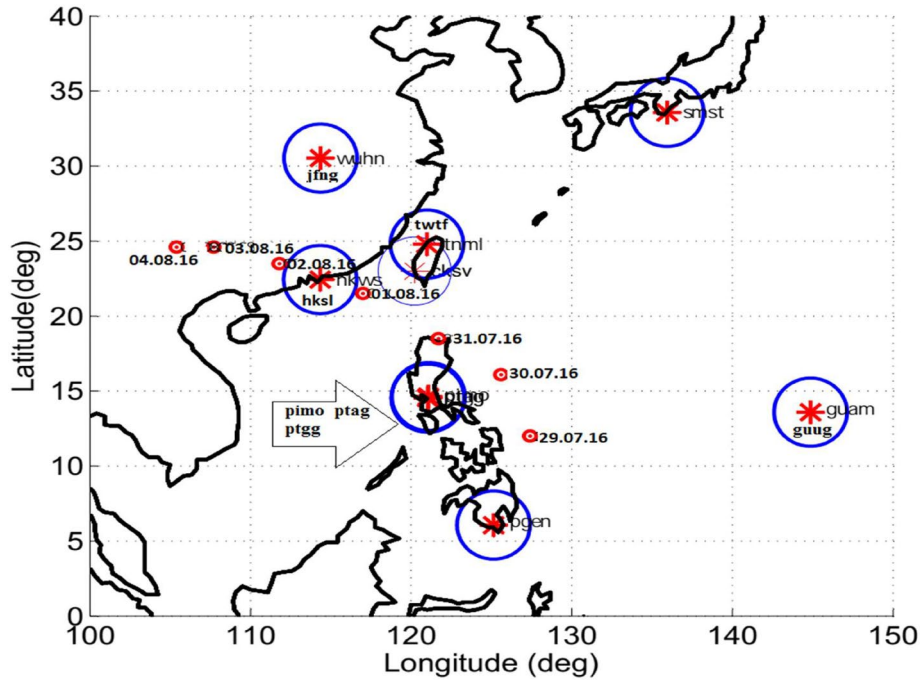

Figure 5. Map showing cyclone track from 29 July to 04 August and GPS stations considered. The cyclone path with date is represented by red circle. The GPS stations are marked by * with red color and each GPS station is rounded by blue circle. These GPS stations are lying left, along and right to cyclone track.

ionospheric altitude and their ionization there (Belyaev et al., 2015). Belyaev et al. (2015) proposed the Model for the formation above TC in the lower ionosphere vertical submerged jet that injects neutral particles of different varieties into the upper ionosphere on ballistic trajectories. Changing of the ionization of neutral particles near the terminator and the deviation of the jet under the interaction of the TC with the island are confirmed in the proposed model. As strong lightning activity is noticed during the cyclone period which can be seen from Figure 4 and lightning induced electric filed helps in redistribution of ionospheric plasma through $\mathbf{E} \times \mathbf{B}$ electro-dynamical drift which lift the plasma toward higher altitude where loss is less significant. The inclusion of data of drift measurement to this paper is useful to explain the results more clearly. In addition, TC landfall is normally associated with the change in electromotive force of global atmosphere-ionosphere circuit by variation of wind and charge aerosols density. Consequently, this variation leads to change in the electric field in the atmosphere-ionosphere system. High wind speed (158 km/hr) noticed during the cyclone may affect the magnitude of electro-motive force (Electric field) which may also affect the ionospheric electron density. The observation of DC electric field with magnitude up to 20 mV/m in the upper ionosphere over tropical cyclone zone reported by Sorokin et al. (2005). The electrodynamical model reported by Sorokin et al. (2001) indicates that electromagnetic and plasma phenomenon before TC and earthquakes could be visible by means of atmosphere-ionosphere coupling by amplification of DC electric field in the ionosphere over disturbed area. To start these phenomena at the level of the ionosphere the electric field at altitude of the ionosphere should reach a threshold value of 10 mV/m.

Table 1
List of GPS Stations and Their Latitude, Longitude Considered for Study and Maximum Ionospheric Perturbation (TECU)

IGS station code	Latitude	Longitude	Maximum ionospheric perturbation (±TECU)
PGEN	06.06°N	125.13°E	8 TECU
PPPC	9.77°N	118.74°E	4 TECU
PIMO	14.63°N	121.07°E	4 TECU
PTAG	14.53°N	121.04°E	5 TECU
PTGG	14.53°N	121.04°E	7 TECU
GUAM	13.58°N	144.86°E	6 TECU
GUUG	13.43°N	144.80°E	7 TECU
HKSL	22.37°N	113.92°E	9 TECU
HKWS	22.43°N	114.33°E	10 TECU
TNML	24.79°N	120.98°E	6 TECU
TWTF	24.95°N	121.65°E	2 TECU
CKSV	22.99°N	120.22°E	8 TECU
JFNG	30.51°N	114.49°E	3 TECU
WUHN	30.53°N	114.35°E	3 TECU
SMST	33.57°N	135.93°E	10 TECU

During the landfall of cyclone reduction in TEC is noticed at many GPS stations. In recent years cyclonic storms have been well known to produce perturbation in the ionospheric parameters which are reported by several researchers (Dube et al., 2020; Guha et al., 2016). Guha et al. (2016) have studied tropical cyclone effects on the ionosphere and reported decrease in TEC during the landfall of TC. In contrast, our results show decrease as well as increase in TEC observed

at several stations during landfall of TC. From the above results it has been noticed that the response of the ionosphere to cyclone observed from stations lying in eastward direction to the cyclone track is different than that from thosein westward to cyclone track. This could be due to effect of coriolis force because it deflects the winds toward eastward in the Northern hemisphere and westward in the southern hemisphere (Lutgens & Tarbuck, 2013).

3.3. Gravity Waves Signatures

As already stated, convection activity during thunderstorms or typhoons could result in the formation of gravity waves (Kumar et al., 2017). Gravity wave signatures during the passage of the typhoon were detected as follows; First, a Savitzky-Golay filter of order 6 and a window length of 120 min was fitted to the TEC (Osei-Poku et al., 2021). DTEC was obtained by subtracting the fitted TEC from the original TEC. Then, a bi-directional band pass filter of 1–2.8 mHz is applied to the DTEC to obtain the gravity wave signals. Signals above the amplitude of 0.08 TECu were regarded to be gravity waves (Liu et al., 2021; Rahmani et al., 2020). Also, continuous wavelet transform (CWT) was applied to DTEC data to obtain the frequency and period of gravity waves. Gravity waves usually have a frequency of 1–2 mHz and a period of 9–20 min.

Figure 10 shows that gravity waves were generated during the passage of the typhoon as the amplitude of the band pass-filtered DTEC exceeded 0.08TECu. Table 2 is a summary of the frequency, period, propagation distance, and speed of the gravity waves. Propagation distance and speed of the gravity waves have been computed using formulas which can be found in Liu et al. (2021). As reflected from Table 2, the speed of GWs are noted to vary from 74 to 131 $ms^{-1}$with an average of 101 ms^{-1}. Using ERA5 reanalysis data along with air glow measurements, the propagation characteristics of GWs generated during typhoon were studied by Li et al. (2022) they reported the average horizontal wavelength ∼96 km, and the average observed phase velocity ∼90 m s^{-1}.

This observation provides further evidence for gravity waves' contribution to the perturbation in the ionosphere. The signatures of gravity waves in ionosphere due to thunderstorm activity were reported by several workers (Kumar et al., 2017; Li et al., 2022). The periods of observed GWs from 9 to 20 min and to frequency 1–2 mHz were reported. In addition to cyclone activities, other phenomenon in lower atmosphere can also be responsible for generation of GWs. These include solar eclipse, earthquakes, tropospheric turbulence, jet flows, thunderstorms, weather fronts etc (Kumar et al., 2021). Depending on sources periods of GWs vary from 10 min to 3 hr. The seismic induced GWs signatures are also present in ionosphere with period from 15 to 60 min and horizontal wavelength of several hundred kms which are reported by previous workers (Hocke & Schlegel, 1996; Oikonomou et al., 2016). Using the band pass filter technique to GNSS carrier phase observation in China, Liu et al. (2021) reported period of thunderstorm induced GWs from 6 to 20 min. They have further shown 0.2–0.8 TECU perturbation in TEC data when trajectory of IPP falls into the perturbed region and period below 6 min and above 20 min such perturbation is not considered as GWs. In the present investigation only GPS-TEC data of ionosphere have been used which cannot reflects altitude information. The tropical cyclones are capable to generate concentric gravity waves in troposphere which can propagates toward upper atmosphere creates disturbances and period of such GWs changes during their propagation which changes with altitude (Zhao et al., 2020). To identify the source of GWs and their propagation characteristics, data from tropospheric altitudes are required. In this paper due to absence of such data, source of cyclone induced GWs could not be identified. The source of GWs can be identified using data of temperature and wind field measurement from sounding as reported by He et al. (2020) in North Western China. They have shown that buoyancy frequency increases over 10.5–13 km altitude and average buoyancy frequency in troposphere (below 10 km) is about 0.0076 rad/s (∼1 mHz). Buoyancy frequency or Brunt–Väisälä frequency is the frequency at which vertically displaced air parcel will oscillate which can be measured from gradient in potential temperature. The waves which are at or below the buoyancy frequency is not considered as a gravity waves. In this paper detection of waves of frequency 1–2 mHz, period 9–20 min, propagation velocity ∼74–131 ms^{-1} at ionospheric altitude are noticed during cyclone period, which may be GWs.

3.4. Observation of Plasma Bubbles and Scintillation

3.4.1. Observation From GPS

The presence of ionospheric irregularities/plasma bubbles causes fluctuation amplitude and phase of the GPS signals while passing through them, known as scintillation. The strength of amplitude scintillation in GPS signal is measured by S_4 index which is defined as the ratio of standard deviation of the signal power/intensity to

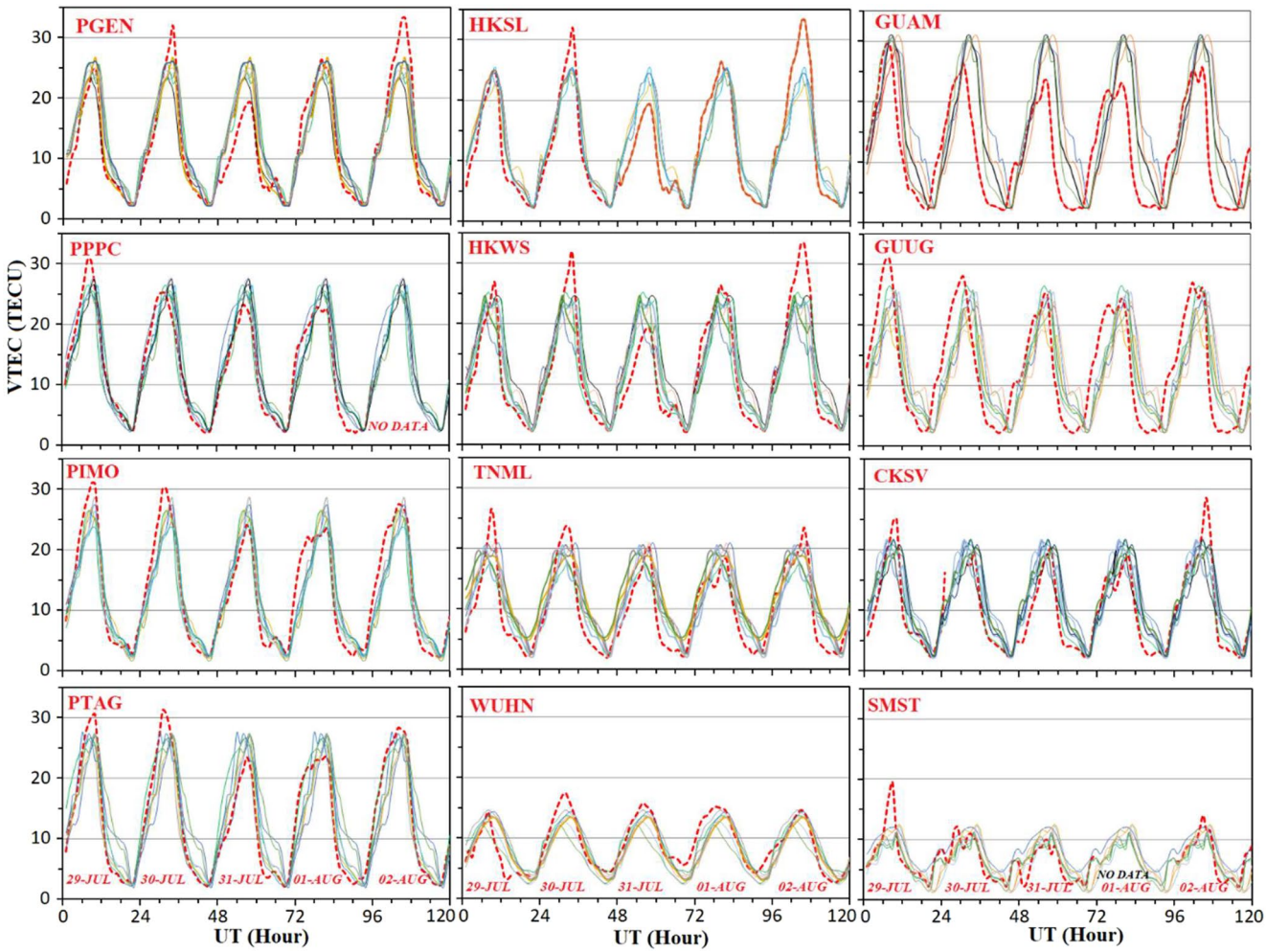

Figure 6. Variation of TEC during cyclone period (red dotted line) from 29 July to 02 August 2016 along with TEC *during geomagnetic quiet days of the month* (solid line) at stations PGEN, PPPC, PIMO, PTAG, HKSL, HKWS, TNML, WUHN, GUAM, GUUG, CKSV, SMST.

the mean signal power computed over a period of 60 s (1 min). The amplitude scintillation index (S_4) is also computed from the GPS station at Sanya in China during cyclone period from 30 July to 03 August. Figure 7 shows variation of S_4-index from PRN 25 at Sanya Station in China. From this figure S_4-index during cyclone period on 01 and 02 August go beyond 0.5 showing strong scintillation activity in GPS signal and presence of ionospheric irregularities. The S_4-index is noted to be maximum of 1.35 on 02 August observed during 1400–1600 UT. In addition to S4-index ROTI for PRN 25 at Sanya station is also computed during the period from

Table 2
Gravity Wave Parameters During the Passage of Typhoon Nida

Day	Station	Frequency (mHz)	Period (minutes)	Propagation distance (km)	Speed (m/s)
29th July	PIMO (PRN 13)	1.8	8	436	96
30th July	PIMO (PRN 20)	1.3	8.2	392	80
31st July	PIMO (PRN 20)	1.04	15	871	74
1st August	TNML (PRN 20)	0.9	17	1,015	131
2nd August	TNML (PRN 20)	0.9	17	1,015.2	120
3rd August	WUHN (PRN 20)	1.37	11.64	630.74	99.03
4th August	WUHN (PRN 15)	2.5	11.64	630.74	107.99

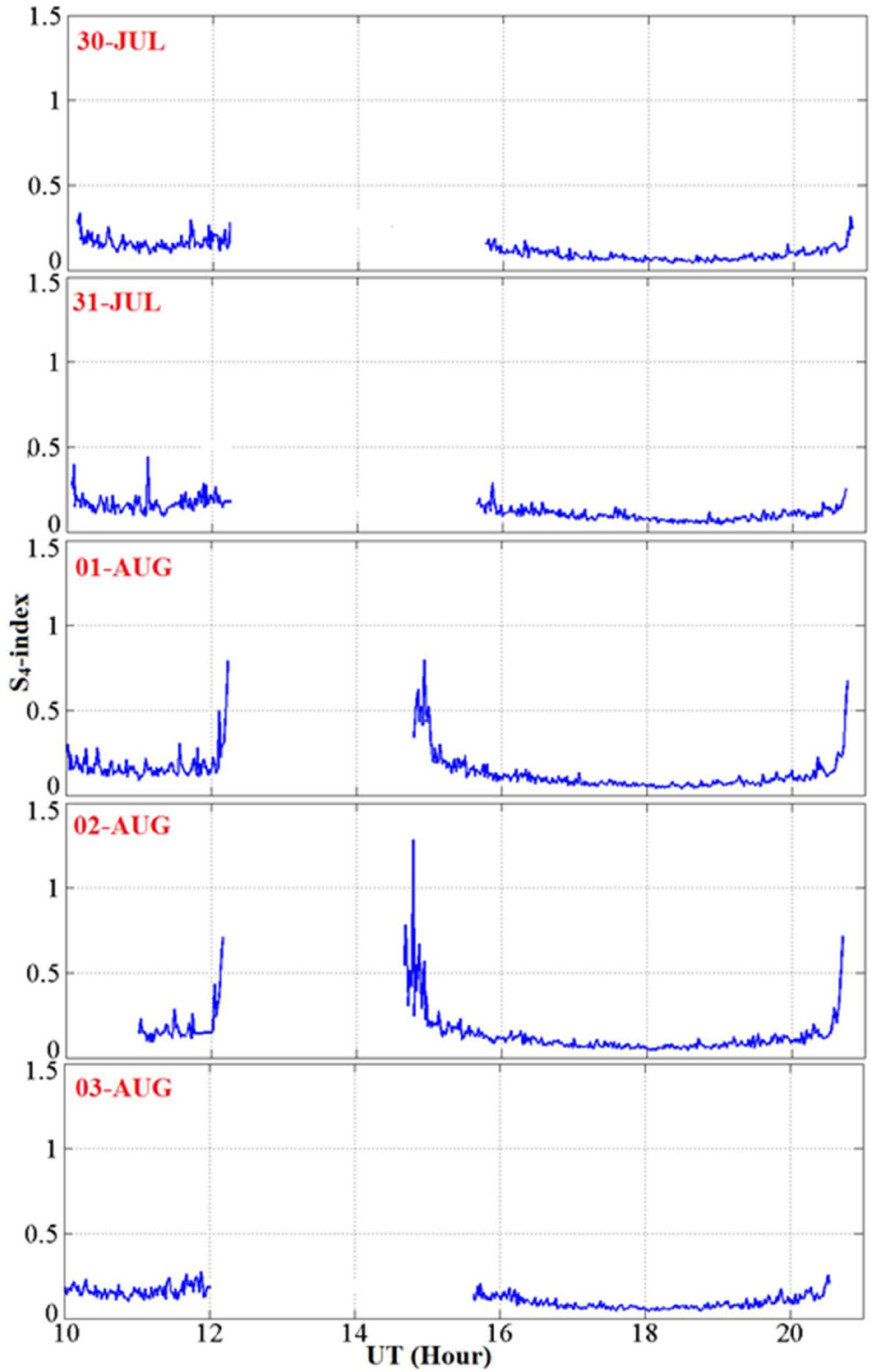

Figure 7. Variation of S_4-index (amplitude scintillation index) derived from PRN 25 during 30 July–03–August 2016 over Sanya GPS station in China which is around km away from cyclone path. In this analysis elevation cut off 20° is taken into account. S4-index during cyclone period on 01 and 02 August go beyond 0.5 with a maximum value of 1.35 on 02 August.

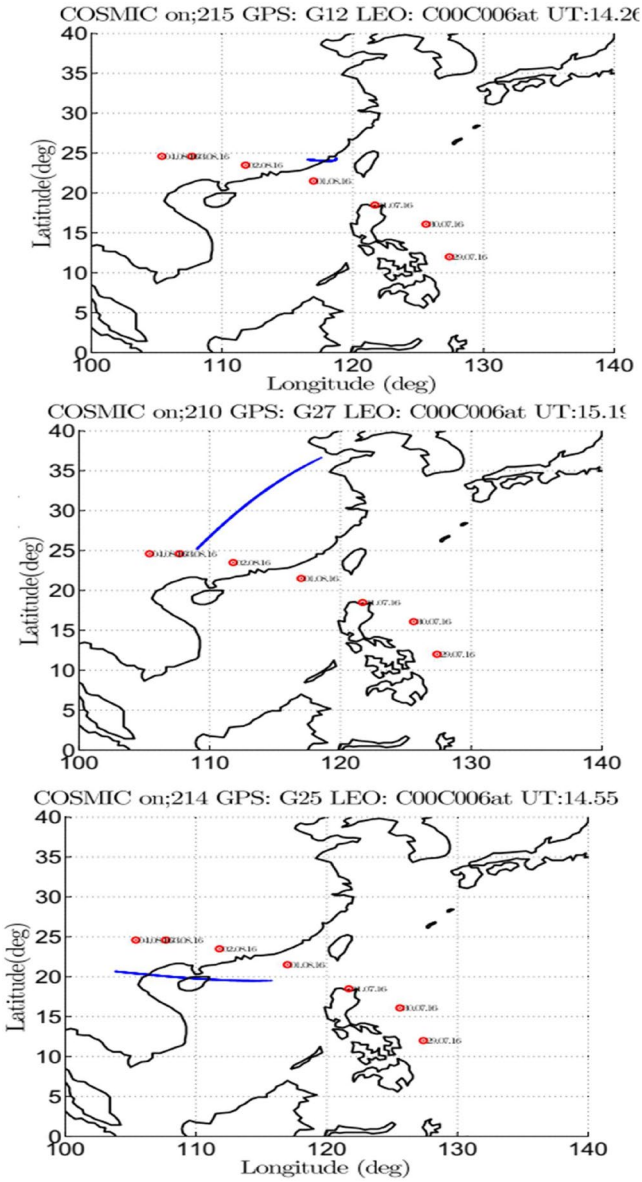

Figure 8. Trajectory indicating location of measurements plotted using latitude/longitude of tangent points along the ray connecting COSMIC LEO with respective GPS satellite during cyclone period on 28 July, 01 August, and 02 August.

30 July to 03 August 2016. The ROTI is also an indicator of presence of ionospheric irregularities/plasma bubbles. In addition to S4-index, the rate of TEC change index (ROTI) during cyclone are also analyzed and found that ROTI during period of cyclone found greater than 0.5 with a maximum (ROTI ~ 1.6) on 02 August 2016. The difference of ROTI during evening and daytime is related to scintillation activity and ROTI = 0.075 TECU/min can be used as a threshold for scintillation activity in GPS signal (Nishioka et al., 2008).

3.4.2. Observation From COSMIC

To confirm the presence of scintillation activity on 01 and 02 August 2016 as observed from GPS-based ground observation at Sanya station, satellite based observation from COSMIC (Constellation observing system from meteorology ionosphere and climate) is also considered. COSMIC also takes measurements from the GPS satellite and receiver is on board on LEO (Low Earth Orbiting) satellite. Figure 8 shows the trajectory of LEO satellite of COSMIC which was passing near the cyclone track on 28 July 01 August and 02 August. Trajectories have been drawn using location of measurements: latitude/longitude of tangent points along the ray connecting COSMIC LEO with respective GPS satellite. The amplitude scintillation index S4-index from COSMIC is analyzed during the cyclone period. As seen from Figure 8, three COSMIC trajectories were passed near the cyclone track during the cyclone period which used GPS satellites id G12, G27, and G22 in track with LEO satellite id C006. The S4-index data analyzed from these three satellites during the cyclone period is shown in Figure 9. From Figure 9 it is seen that COSMIC based measurements also show strong scintillation activity (S_4-index > 0.8) during the cyclone period which was observed on 01 and 02 August. Moreover, the observed S_4-index from COSMIC maximized during 1400–1600 UT hr and same has also observed from the GPS based measurement.

Using data from Jicamarca Radio Observatory Woodman and Kudeki (1984) proposed that the increased electric field from thunderstorm activity may lead to plasma instability and plasma bubble in F region ionosphere. Thunderstorm activity as well as deep convection observed during the cyclone period may generate GWs which propagates upward (Chou et al., 2016; Taylor et al., 2009; Vadas et al., 2009). The upward propagating GWs acts as seeds in the Mesosphere which is required for the development of Rayleigh-Taylor instability (Taylor et al., 2009; Vadas et al., 2009) and generation of plasma bubbles and equatorial spread F in the ionosphere which further produces scintillation in radio signal while passing through them (Vadas & Fritts, 2004). Using data from ground GPS and COSMIC satellite for 2012 tropical Tembin cyclone, Yang and Liu (2016) reported strong scintillation activity in GPS and COSMIC signals over Hong Kong region on the quiet day of 26 August 2012 when cyclone passed close to the Hong Kong. They suggested that the scintillation activity could have been caused by plasma irregularities triggered by the gravity wave generated in the troposphere during cyclone period.

4. Summary and Conclusion

Our analysis presents observation on the effects of tropical cyclone Nida on atmosphere and ionosphere. To study the atmospheric and ionospheric perturbations ground and satellite based data from GPS, COSMIC, and AIRS satellite have been analyzed. Results of the present study are summarized below:

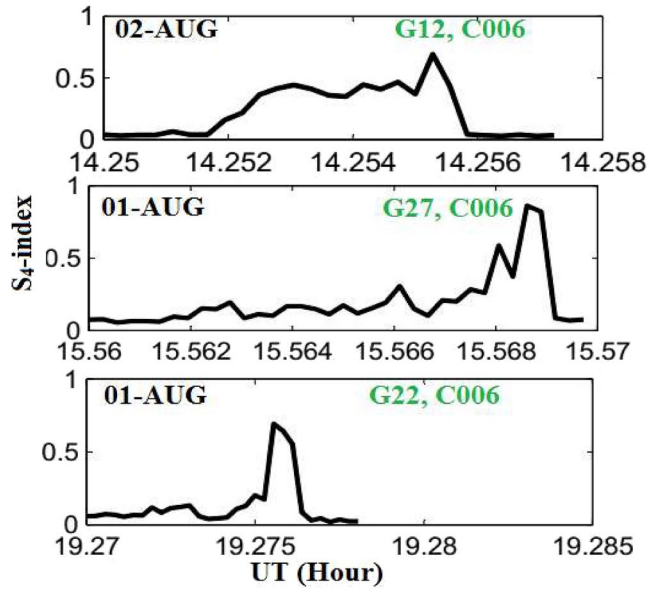

Figure 9. Variation of S4-index (amplitude scintillation index) derived from COSMIC passing near cyclone path on 01 August (with GPS PRN 22 and 27) and 02 August (with GPS PRN 12).

Analysis of TOC data from AIRS satellite during the cyclone period indicates significant enhancement in atmospheric ozone observed during the cyclone period. The enhancement in TOC could be attributed to thunderstorm activity present during the cyclone period (Figure 4) which is known to be a source of NOx which further affects the production of ozone through chemical reactions. Since, the effect of Coriolis force over mid and high latitude is more significant as compared to the equatorial and tropical region which deflects the wind toward eastward (westward) in the Northern (Southern) hemisphere, therefore spatial and vertical distribution of ozone will show better picture and is recommended for further investigation (Lutgens & Tarbuck, 2013). The enhanced ozone density observed during the cyclone period controls the ionization balance in the lower D-region which may affect the ionosphere (Macotela et al., 2019; Osepian & Dalin 2009).

The analysis of the TEC data was performed during the period of TC which was free from the solar and geomagnetic activity and is suitable for detection of ionospheric perturbations from cyclone activity. Analysis found perturbation in the ionosphere depends on the location of observing station from the cyclone path. The stations lying on the right side/eastward from the cyclone path shows different behavior than that lying on westward which could be caused by the effect of Coriolis force. In addition to decrease in TEC, an enhancement is also observed at several stations during landfall of TC which is in contrast to the results of Guha et al. (2016) who have shown decrease in TEC during landfall of TC. The ionospheric perturbations could be caused by thunderstorm-induced electric filed as observed during the cyclone period which supports the plasma redistribution through the $\mathbf{E} \times \mathbf{B}$ electrodynamics drift. Although data of plasma drift is useful to support the present result but in the absence of such data present observations could not be clearly explained.

Ionspheric scintillation is also analyzed during TC using data from ground based GPS measurements as well as radio occultation technique that is, from COSMIC. Both the data sets reveal presence of strong scintillation activity during cyclone period having amplified magnitude as compared to those observed without TC. The observed scintillation found to be maximum on 01 and 02 August during 1400–1600 UT. The presence of plasma bubbles and scintillation activity of amplified magnitude observed during the TC could be caused by thunderstorm/lightning induced electric field as well as gravity waves generated due to deep convection activity (Taylor et al., 2009; Vadas et al., 2009; Woodman & Kudeki, 1984). The detection of GWs of frequency 1–2 mHz, period 9–20 min with propagation velocity ~74–131 ms^{-1} at altitude of ionosphere are noticed during cyclone period which may be gravity waves but present study could not identify source of such GWs due to lack of tropospheric measurements. However measurements and results of other worker indicate its source to be in the troposphere (He et al., 2020; Zhao et al., 2020).

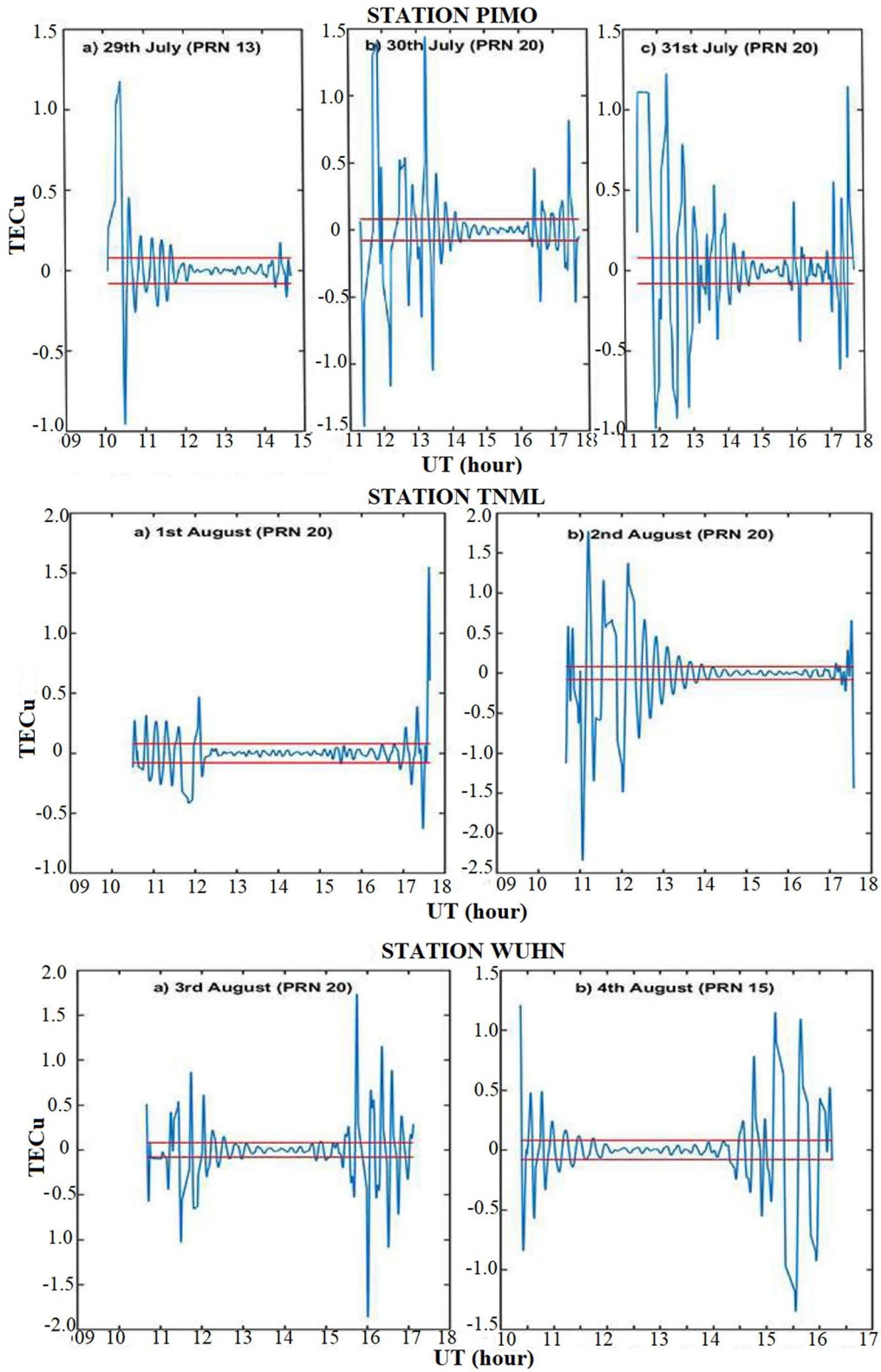

Figure 10. Detection of Gravity Waves during the passage of Typhoon Nida. Red Lines show the threshold of 0.08TECu.

Data Availability Statement

The total ozone column (TOC) data from AIRS satellite has been taken from GIOVANI website interfaced at https://giovanni.gsfc.nasa.gov/giovanni/. GPS data in RINEX format used in this study have been downloaded from IGS website which are openly available at cddis.gsfc.nasa.gov. Solar and geomagnetic data have been taken from OMNIWEB at omniweb.gsfc.nasa.gov.

Acknowledgments
This research is partially supported by the research fund from Research Institute of Land Space of the Hong Kong Polytechnic University. Authors thank to the anonymous reviewer for their constructive comments/suggestions which helped to improve MS quality.

References

Belyaev, G., Boychev, B., Kostin, V., Trushkina, E., & Ovcharenko, O. (2015). Modification of the ionosphere near the terminator due to the passage of a strong tropical cyclone through the large Island. *Sun and Geosphere*, *10*, 31–38.

Bourqui, M. S., & Trepanier, P. Y. (2010). Descent of deep stratospheric intrusions during the IONS August 2006 campaign. *Journal of Geophysical Research*, *115*(D18), D18301. https://doi.org/10.1029/2009JD013183

Cairo, F., Buontempo, C., MacKenzie, A. R., Schiller, C., Volk, C. M., Adriani, A., et al. (2008). Morphology of the tropopause layer and lower stratosphere above a tropical cyclone: A case study on cyclone Davina. *Atmospheric Chemistry and Physics*, *8*(13), 3411–3426. https://doi.org/10.5194/acp-8-3411-2008

Chou, C.-C., Dai, J., Kuo, C.-L., & Huang, T.-Y. (2016). Simultaneous observations of storm-generated sprite and gravity wave over Bangladesh. *Journal of Geophysical Research: Space Physics*, *121*(9), 9222–9233. https://doi.org/10.1002/2016JA022554

Collier, A. B., Hughes, A. R. W., Lichtenberger, J., & Steinbach, P. (2006). Seasonal and diurnal variation of lightning activity over southern Africa and correlation with European whistler observations. *Annales Geophysicae*, *24*(2), 529–542. https://doi.org/10.5194/angeo-24-529-2006

Das, S. S., Ratnam, M. V., Uma, K. N., Subrahmanyam, K. V., Girach, I. A., Patra, A. K., et al. (2016). Influence of tropical cyclones on tropospheric ozone: Possible implications. *Atmospheric Chemistry and Physics*, *16*(8), 4837–4847. https://doi.org/10.5194/acp-16-4837-2016

Dube, A., Singh, R., Maurya, A. K., Kumar, S., Sunil, P. S., & Singh, A. K. (2020). Ionospheric perturbations induced by a very severe cyclonic storm (VSCS): A case study of Phailin VSCS. *Journal of Geophysical Research: Space Physics*, *125*(1), e2019JA027197. https://doi.org/10.1029/2019JA027197

Forbes, J. M., Palo, S. E., & Zhang, X. (2000). Variability of the ionosphere. *Journal of Atmospheric and Solar-Terrestrial Physics*, *62*(8), 685–693. https://doi.org/10.1016/s1364-6826(00)00029-8

Fritts, D. C., & Alexander, M. J. (2003). Gravity wave dynamics and effects in the middle atmosphere. *Reviews of Geophysics*, *41*(1), 1003. https://doi.org/10.1029/2001RG000106

Fritts, D. C., & Nastrom, G. D. (1992). Sources of mesoscale variability of gravity waves, II, frontal, convective and jet stream excitation. *Journal of the Atmospheric Sciences*, *49*(2), 111–127. https://doi.org/10.1175/1520-0469(1992)049<0111:somvog>2.0.co;2

Guha, A., Paul, B., Chakraborty, M., & De, B. K. (2016). Tropical cyclone effects on the equatorial ionosphere: First result from the Indian sector. *Journal of Geophysical Research: Space Physics*, *121*(6), 5764–5777. https://doi.org/10.1002/2016JA022363

He, Y., Sheng, Z., & He, M. (2020). Spectral analysis of gravity waves from near space high-resolution Balloon data in Northwest China. *Atmosphere*, *11*(2), 133. https://doi.org/10.3390/atmos11020133

Hocke, K., & Schlegel, K. (1996). A review of atmospheric gravity waves and travelling ionospheric disturbances: 1982-1995. *Annales Geophysicae*, *14*(9), 917–940. https://doi.org/10.1007/s00585-996-0917-6

Holton, J. R., Haynes, P. T., Mclntyre, M. E., Douglass, A. R., Rood, R. B., & Pfister, L. (1995). Stratospheretroposphere exchange. *Reviews of Geophysics*, *33*(4), 403–439. https://doi.org/10.1029/95RG02097

Immel, T. J., Mende, S. B., Hagan, M. E., Kintner, P. M., & England, S. L. (2009). Evidence of tropospheric effects on the ionosphere. *Eos, Transactions American Geophysical Union*, *90*(9), 69–80. https://doi.org/10.1029/2009EO090001

Isaev, N. V., Sorokin, V. M., Chmyrev, V. M., Serebryakova, O. N., & Ovcharenko, O. Y. (2002). Electric field enhancement in the ionosphere above tropical stormregion. In M. Hayakawa, & O. A. Molchanov (Eds.), *Seismo electromagnetics: Lithosphere–atmosphere–ionosphere coupling* (pp. 313–315). TERRAPUB.

Isaev, N. V., Sorokin, V. M., Chmyrev, V. M., Serebryakova, O. N., & Yaschenko, A. K. (2002). Disturbance of the electric field in the ionosphere by sea storms and typhoons. *Cosmic Research*, *40*(6), 547–553. https://doi.org/10.1023/A:1021549612290

Isaev, N. V., Sorokin, V. M., Serebryakova, O. N., Stanev, G. A., Yaschenko, A. K., & Trushkina, E. P. (2006). Electric field enhancement and disturbances of plasma density in the ionosphere above the zones of preparation and development of typhoons. *Space, Ecology, Nanotechnology, Safety, Varna, Bulgaria*.

Kumar, S., Chen, W., Chen, M., Liu, Z., & Singh, R. P. (2017). Thunderstorm-/lightning-induced ionospheric perturbation: An observation from equatorial and low-latitude stations around Hong Kong. *Journal of Geophysical Research: Space Physics*, *122*(8), 9032–9044. https://doi.org/10.1002/2017JA023914

Kumar, S., Tripathi, G., Kumar, P., Singh, A. K., & Singh, A. K. (2021). Ionospheric perturbations observed due to Indonesian Earthquake (Mw = 7.4) using GPS and VLF measurements at multi-stations. *Acta Geodaetica et Geophysica*, *56*(3), 559–577. https://doi.org/10.1007/s40328-021-00345-5

Kuo, C. L., & Lee, L. C. (2015). Ionospheric plasma dynamics and instability caused by upward currents above thunderstorms. *Journal of Geophysical Research: Space Physics*, *120*(4), 3240–3253. https://doi.org/10.1002/2014JA020767

Lastovicka, J. (2006). Forcing of the ionosphere by waves from below. *Journal of Atmospheric and Solar-Terrestrial Physics*, *68*(3–5), 479–497. https://doi.org/10.1016/j.jastp.2005.01.018

Lay, E. H., Shao, X., Kendrick, A. K., & Carrano, C. S. (2015). Ionospheric acoustic and gravity waves associated with midlatitude thunderstorms. *Journal of Geophysical Research: Space Physics*, *120*(7), 6010–6020. https://doi.org/10.1002/2015JA021334

Li, Q., Xu, J., Liu, H., Liu, X., & Yuan, W. (2022). How do gravity waves triggered by a typhoon propagate from the troposphere to the upper atmosphere? *Atmospheric Chemistry and Physics*, *22*(18), 12077–12091. https://doi.org/10.5194/acp-22-12077-2022

Liu, T., Yu, Z., Ding, Z., Nie, W., & Xu, G. (2021). Observation of ionospheric gravity waves introduced by thunderstorms in low latitudes China by GNSS. *Remote Sensing*, *13*(20), 4131. https://doi.org/10.3390/rs13204131

Lutgens, F. K., & Tarbuck, E. J. (2013). The atmosphere: An introduction to meteorology (12th ed., pp. 170–172).

Macotela, E. L., Clilverd, M. A., Manninen, J., Thomson, N. R., Newnham, D. A., & Raita, T. (2019). The effect of ozone shadowing on the D region ionosphere during sunrise. *Journal of Geophysical Research: Space Physics*, *124*(5), 3729–3742. https://doi.org/10.1029/2018ja026415

Naik, H., Naqvi, S. W. A., Suresh, T., & Narvekar, P. V. (2008). Impact of a tropical cyclone on biogeochemistry of the central Arabian Sea. *Global Biogeochemical Cycles*, *22*(3), GB3020. https://doi.org/10.1029/2007gb003028

Nastrom, G. D., & Fritts, D. C. (1992). Sources of mesoscale variability of gravity waves.1. Topographic excitation. *Journal of the Atmospheric Sciences*, *49*(2), 101–110. https://doi.org/10.1175/1520-0469(1992)049<0101:somvog>2.0.co;2

Nishioka, M., Saito, A., & Tsugawa, T. (2008). Occurrence characteristics of plasma bubble derived from global ground-based GPS receiver networks. *Journal of Geophysical Research*, *113*(A5), A05301. https://doi.org/10.1029/2007JA012605

Oikonomou, C., Haralambous, H., & Muslim, B. (2016). Investigation of ionospheric TEC precursors related to the M78 Nepal and M83 Chile earthquakes in 2015 based on spectral and statistical analysis. *Natural Hazards*, *83*(S1), 97–116. https://doi.org/10.1007/s11069-016-2409-7

Osei-Poku, L., Tang, L., Chen, W., & Mingli, C. (2021). Evaluating total electron content (TEC) detrending techniques in determining ionospheric disturbances during lightning events in A low latitude region. *Remote Sensing*, *13*(23), 4753. https://doi.org/10.3390/rs13234753

Osepian, A. S. K., & Dalin, P. (2009). The influence of ozone concentration on the lower ionosphere –modelling and measurements during the 29–30 October 2003 solar proton event. *Annales Geophysicae*, *27*(2), 577–589. https://doi.org/10.5194/angeo-27-577-2009

Parkinson, C. L. (2003). Aqua: An Earth-observing satellite mission to examine water and other climate variables. *IEEE Transactions on Geoscience and Remote Sensing*, *41*(2), 173–183. https://doi.org/10.1109/tgrs.2002.808319

Pi, X., Mannucci, A. J., Lindqwister, U. J., & Ho, C. M. (1997). Monitoring of global ionospheric irregularities using the Worldwide GPS Network. *Geophysical Research Letters*, *24*(18), 2283–2286. https://doi.org/10.1029/97GL02273

Polyakova, A. S., & Perevalova, N. P. (2011). Investigation into impact of tropical cyclones on the ionosphere using GPS sounding and NCEP/NCAR reanalysis data. *Advances in Space Research*, *48*(7), 1196–1210. https://doi.org/10.1016/j.asr.2011.06.014

Rahmani, Y., Alizadeh, M. M., Schuh, H., Wickert, J., & Tsai, L.-C. (2020). Probing vertical coupling effects of thunderstorms on lower ionosphere using GNSS data. *Advances in Space Research*, *66*(8), 1967–1976. https://doi.org/10.1016/j.asr.2020.07.018

Rama Rao, P. V. S., Gopi Krishna, S., Niranjan, K., & Prasad, D. S. V. V. D. (2006). Temporal and spatial variations in TEC using simultaneous measurements from the Indian GPS network of receivers during the low solar activity period of 2004–2005. *Annales Geophysicae*, *24*(12), 3279–3292. https://doi.org/10.5194/angeo-24-3279-2006

Shao, X.-M., Lay, E. H., & Jacobson, A. R. (2013). Reduction of electron density in the night-time lower ionosphere in response to a thunderstorm. *Nature Geoscience*, *6*(1), 29–33. https://doi.org/10.1038/ngeo1668

Shen, C. S. (1982). The correlations between the typhoon and the foF2 of ionosphere. *Chinese Journal of Space Science*, *2*, 335–340.

Sorokin, V. M., & Cherny, G. P. (1999). It is quite possible to monitor typhoons from outer space. *Aerospace Courier*, *3*, 84–87.

Sorokin, V. M., Chmyrev, G. P., & Yaschenko, A. (2001). Electrodynamic model of lower atmosphere and the ionosphere coupling. *Journal of Atmospheric and Solar-Terrestrial Physics*, *63*(16), 1681–1691. https://doi.org/10.1016/s1364-6826(01)00047-5

Sorokin, V. M., Isaev, N. V., Yaschenko, A. K., Chmyrev, V. M., & Hayakawac, M. (2005). Strong DC electric field formation in the low latitude ionosphere over typhoons. *Journal of Atmospheric and Solar-Terrestrial Physics*, *67*(14), 1269–1279. https://doi.org/10.1016/j.jastp.2005.06.014

Stohl, A., Wernli, H., Bourqui, M., Forster, C., James, P., Liniger, M. A., et al. (2003). A new perspective of stratosphere-troposphere exchange. *Bulletin of the American Meteorological Society*, *84*(11), 1565–1573. https://doi.org/10.1175/BAMS-84-11-1565

Takahashi, H., Taylor, M. J., Pautet, P. D., Medeiros, A. F., Gobbi, D., Wrasse, C. M., et al. (2009). Simultaneous observation of ionospheric plasma bubbles and mesospheric gravity waves during the SpreadFEx Campaign. *Annales Geophysicae*, *27*(4), 1477–1487. https://doi.org/10.5194/angeo-27-1477-2009

Tang, L., Chen, W., Chen, M., & Louis, O.-P. (2019). Statistical observation of thunderstorm-induced ionospheric Gravity waves above low-latitude areas in the Northern Hemisphere. *Remote Sensing*, *11*(23), 2732. https://doi.org/10.3390/rs11232732

Tang, L., Louis, O.-P., Chen, W., & Chen, M. A. (2021). ROTI-aided equatorial plasma bubbles detection method. *Remote Sensing*, *13*(21), 4356. https://doi.org/10.3390/rs13214356

Taylor, M. J., Pautet, P.-D., Medeiros, A. F., Buriti, R., Fechine, J., Fritts, D. C., et al. (2009). Characteristics of mesospheric gravity waves near the magnetic equator, Brazil, during the SpreadFEx campaign. *Annales Geophysicae*, *27*(2), 461–472. https://doi.org/10.5194/angeo-27-461

Vadas, S. L., & Azeem, I. (2021). Concentric secondary gravity waves in the thermosphere and ionosphere over the continental United States on 25–26 March 2015 from deep convection. *Journal of Geophysical Research: Space Physics*, *126*(2), e2020JA028275. https://doi.org/10.1029/2020JA028275

Vadas, S. L., & Fritts, D. C. (2004). Thermospheric responses to gravity waves arising from mesoscale convective complexes. *Journal of Atmospheric and Solar-Terrestrial Physics*, *66*(6), 781–804. https://doi.org/10.1016/j.jastp.2004.01.025

Vadas, S. L., Taylor, M. J., Pautet, P.-D., Stamus, P. A., Fritts, D. C., Liu, H.-L., et al. (2009). Convection: The likely source of the medium-scale gravity waves observed in the OH airglow layer near Brasilia, Brazil, during the Spread F Ex campaign. *Annales Geophysicae*, *27*(1), 231–259. https://doi.org/10.5194/angeo-27-231-2009

Woodman, R. F., & Kudeki, E. (1984). A causal relationship between lightning and explosive spread F. *Geophysical Research Letters*, *11*(12), 1165–1167. https://doi.org/10.1029/GL011i012p01165

Yang, Z., & Liu, Z. (2016). Observational study of ionospheric irregularities and GPS scintillations associated with the 2012 tropical cyclone Tembin passing Hong Kong. *Journal of Geophysical Research: Space Physics*, *121*(5), 1–13. https://doi.org/10.1002/2016JA022398

Zhao, Y., Deng, Y., Wang, J.-S., Zhang, S.-R., & Lin, C. Y. (2020). Tropical cyclone-induced gravity wave perturbations in the upper atmosphere: GITM-R simulations. *Journal of Geophysical Research: Space Physics*, *125*(7), e2019JA027675. https://doi.org/10.1029/2019ja027675